# LARGE SCALE URBAN SIMULATIONS WITH THE MILES APPROACH

**Gopal Patnaik, Jay P. Boris, and Fernando F. Grinstein**
LCP&FD, Naval Research Laboratory, Washington, DC 20375-5344
**John P. Iselin**
Bucknell University, Lewisburg, PA 17837

**Abstract**

Airborne contaminant transport in cities presents challenging new requirements for CFD. The unsteady flow physics is complicated by very complex geometry, multi-phase particle and droplet effects, radiation, latent, and sensible heating effects, and buoyancy effects. Turbulence is one of the most important of these phenomena and yet the overall problem is sufficiently difficult that the turbulence must be included efficiently with an absolute minimum of extra memory and computing time. This paper describes the Monotone Integrated Large Eddy Simulation (MILES) methodology used in NRL's FAST3D-CT simulation model for urban contaminant transport (CT) (see [1] and references therein). We also describe important extensions of the underlying Flux-Corrected Transport (FCT) convection algorithms to further reduce numerical dissipation in narrow channels (streets).

## 1. Background

Urban airflow accompanied by contaminant transport presents new, extremely challenging modeling requirements. Configurations with very complex geometries and unsteady buoyant flow physics are involved.The widely varying temporal and spatial scales exhaust current modeling capacities. Simulations of dispersion of airborne pollutants in urban scale scenarios must predict both the detailed airflow conditions as well as the associated behavior of the gaseous and multiphase pollutants. Reducing health risks from the accidental or deliberate release of Chemical, Biological, or Radioactive (CBR) agents and pollutants from industrial leaks, spills, and fires motivates this work. Crucial technical issues include transport model specifics, boundary condition modeling, and post-processing of the simulation results for practical use by responders to actualreal-time emergencies.



Relevant physical processes to be modeled include resolving complex building vortex shedding and recirculation zones and representing the associated subgrid scale (SGS) turbulent stochastic backscatter. The model must also incorporate a consistent stratified urban boundary layer with realistic wind fluctuations, solar heating including shadows from buildings and trees, aerodynamic drag and heat losses due to the presence of trees, surface heat sorption variations and turbulent heat transport. Because of the short time spans and large air volumes involved, modeling a pollutant as well mixed globally is typically not appropriate. It is important to capture the effects of unsteady, non-isothermal, buoyant flow conditions on the evolving pollutant concentration distributions. In fairly typical urban scenarios, both particulate and gaseous contaminants behave similarly insofar as transport and dispersion are concerned, so that the contaminant spread can be simulated effectively based on appropriate pollutant tracers with suitable sources and sinks. In other cases the full details of multigroup particle distributions are required.

### *1.1 Established Approach: Gaussian Plume Models*

Contaminant plume prediction technology currently in use throughout the nation is based on Gaussian similarity solutions ("puffs"). This is a class of extended Lagrangian approximations that only really apply for large scales and flat terrain where separated-flow vortex shedding from buildings, cliffs, or mountains is absent. Diffusion is used in plume/puff models to mimic the effects of turbulent dispersion caused by the complex building geometry and wind gusts of comparable and larger size (e.g.,[2-5]). These current aerosol hazard prediction tools for CBR scenarios are relatively fast running models using limited topography, weather and wind data. They give only approximate solutions that ignore the effects of flow encountering 3D structures. The air flowing over and around buildings in urban settings is fully separated. It is characterized by vortex shedding and

turbulent fluctuations throughout the fluid volume. In this regime, the usual timesaving approximations such as steady-state flow, potential flow, similarity solutions, and diffusive turbulence models are largely inapplicable. Therefore a clear need exists for high-resolution numerical models that can compute accurately the flow of contaminant gases and the deposition of contaminant droplets and particles within and around real buildings under a variety of dynamic wind and weather conditions.

### *1.2 Computational Fluid Dynamics Approach*

Since fluid dynamic convection is the most important physical process involved in CBR transport and dispersion, the greatest care and effort should be invested in its modeling. The advantages of the Computational Fluid Dynamics (CFD) approach and representation include the ability to quantify complex geometry effects, to predict dynamic nonlinear processes faithfully, and to handle problems reliably in regimes where experiments, and therefore model validations, are impossible or impractical.

#### *1.2.1 Standard CFD Simulations*

Some "time-accurate" flow simulations that attempt to capture the urban geometry and fluid dynamic details are a direct application of standard (aerodynamic) CFD methodology to the urban-scale problem. An example is the work at Clark Atlanta University where researchers conduct finite element CFD simulations of the dispersion of a contaminant in the Atlanta, Georgia metropolitan area. The finite element model includes topology and terrain data and a typical mesh contains approximately 200 million nodes and 55 million tetrahedral elements [6]. These are grand-challenge size calculations and are run on 1024 processors of a CRAY T3E. Similar approaches are being used by other research groups (e.g., [7,8]). The chief difficulty with this approach for large regions is that they are quite computer intensive and involve severe overhead associated with mesh generation.

#### *1.2.2 The Large-Eddy Simulation Approach*

Capturing the dynamics of all relevant scales of motion, based on the numerical solution of the Navier-Stokes Equations (NSE), constitutes Direct Numerical Simulation (DNS), which is prohibitively expensive for most practical flows at moderate-to-high Reynolds Number (Re). On the other end of the CFD spectrum are the industrial standard methods such as the Reynolds-Averaged Navier-Stokes (RANS) approach, e.g., involving k-$\varepsilon$ models, and other first- and second-order closure methods, which simulate the mean flow and model the effects of all turbulent scales. These are generally unacceptable for urban CT modeling because they are unable to capture unsteady plume dynamics. Large Eddy Simulation (LES) constitutes an effective intermediate approach between DNS and the RANS methods. LES is capable of simulating flow features that cannot be handled with RANS such as significant flow unsteadiness and strong vortex-acoustic couplings, and provides higher accuracy than the industrial methods at reasonable cost.

The main assumptions of LES are: (i) that transport is largely governed by large-scale unsteady convective features that can be resolved, (ii) that the less-demanding accounting of the small-scale flow features can be undertaken by using suitable subgrid scale (SGS) models. Because the larger scale unsteady features of the flow are expected to govern the unsteady plume dynamics in urban geometries, the LES approximation has the potential to capture many key features which the RANS methods and the various Gaussian plume methodologies cannot.

## 2. Monotonically Integrated LES

Traditional LES approaches seek sufficiently high-order discretization and grid resolution to ensure that effects due to numerics are sufficiently small, so that crucial LES turbulence ingredients (filtering and SGS modeling) can be resolved. In the absence of an accepted universal theory of turbulence, the development and improvement of SGS models are unavoidably pragmatic and based on the rational use of empirical information. Classical approaches have included many proposals ranging from, inherently-limited eddy-viscosity formulations, to more sophisticated mixed models combining dissipative eddy-viscosity models with the more accurate but less stable Scale-Similarity Model (SSM), see [9] for a recent survey. The main drawback of mixed models relates to their computational complexity and cost for the practical flows of interest at moderate-to-high Re.

The shortcomings of LES methods have led many researchers to abandon the classical LES formulations and shift focus directly to the SGS modeling implicitly provided by nonlinear (monotone) convection algorithms. (see, e.g., [10], for a recent survey). The idea that a suitable SGS reconstruction might be implicitly provided by

discretization in a particular class of numerical schemes [11] lead to proposing the Monotonically Integrated LES (MILES) approach [12,13]. Later theoretical studies show clearly that certain nonlinear (flux-limiting) algorithms with dissipative leading order terms have appropriate built-in (i.e. "implicit") Sub-Grid Scale (SGS) models [14-16]. Our formal analysis and numerous tests have demonstrated that the MILES implicit tensorial SGS model is appropriate for both free shear flows and wall bounded flows. These are the conditions of most importance for CBR transport in cities.

As discussed further below, the MILES concept can be effectively used as a solid base for CFD-based contaminant transport simulation in urban-scale scenarios, where conventional LES methods are far too expensive and RANS methods are inadequate.

## 3. MILES for Urban Scale Simulations

The FAST3D-CT three-dimensional flow simulation model [1,17,18] is based on the scalable, low dissipation Flux-Corrected Transport (FCT) convection algorithm [19,20]. FCT is a high-order, monotone, positivity-preserving method for solving generalized continuity equations with source terms. The required monotonicity is achieved by introducing a diffusive flux and later correcting the calculated results with an antidiffusive flux modified by a flux limiter. The specific version of the convection algorithm implemented in FAST3D-CT is documented in [21].

Additional physical processes to be modeled include providing a consistent stratified urban boundary layer and realistic wind fluctuations, solar heating including shadows from buildings and trees. We must also model aerodynamic drag and heat losses due to the presence of trees, surface absorption variations and turbulent heat transport. Additional features include multi-group droplet and particle distributions with turbulent transport to surfaces as well as gravitational settling, solar chemical degradation, evaporation of airborne droplets, relofting of particles on the ground and ground evaporation of liquids. Incorporating specific models for these processes in the simulation codes is a challenge but can be accomplished with reasonable sophistication. The primary difficulty is the effective calibration and validation of all these physical models since much of the input needed from field measurements of these processes is typically insufficient or even nonexistent. Furthermore, even though the individual models can all be validated to some extent, the larger problem of validating the overall code has to be tackled as well. Some of principally fluid dynamics related issues are elaborated further below.

### *3.1 Urban Flow Modeling Issues*

#### 3.1.1 *Atmospheric Boundary Layer Specification*

We have to deal with a finite domain and the precise planetary boundary layer characterization upstream of this domain greatly affects the boundary-condition prescription required in the simulations. The weather, time-of-day, cloud cover and humidity all determine if the boundary layer is thermally stable or unstable and thus determine the level and structure of velocity fluctuation. Moreover, the fluctuating winds, present in the real world but usually not known quantitatively except perhaps as a global variance, are known to be important because of sensitivity studies.

In FAST3D-CT the time average of the urban boundary layer is specified analytically with parameters chosen to represent the overall thickness and inflection points characteristic of the topography and buildings upstream of the computational domain. These parameters can be determined self-consistently by computations over a wider domain, since the gross features of the urban boundary layer seem to establish themselves in a kilometer or so, but this increases the cost of simulations considerably.

A deterministic realization of the wind fluctuations is currently being superimposed on the average velocity profiles. This realization is specified as a suitable nonlinear superposition of modes with several wavelengths and amplitudes. Significant research issues remain unresolved in this area, both observationally and computationally. Deterministic [22] and other [23] approaches to formulating turbulent inflow boundary conditions are currently being investigated in this context. The strength of the wind fluctuations, along with solar heating as described just below, are shown to be major determinants of how quickly the contaminant density decreases in time and this in turn is extremely important in emergency applications as it determines overall dosage.

#### *3.1.2 Solar Heating Effects*

An accurate ray-tracing algorithm that properly respects the building and tree geometry computes solar heating in FAST3D-CT. The trees and buildings cast shadows depending on the

instantaneous angle to the sun. Reducing the solar constant slightly can represent atmospheric absorption above the domain of the simulation and the model will even permit emulating a time-varying cloud cover. The geometry database has a land-use variable defining the ground composition. Our simulations to date identify only two conditions, ground and water, though the model can deal with the differences between grass, dirt, concrete and blacktop given detailed enough land-use data. The simulated interaction of these various effects in actual urban scenarios has been extensively illustrated in [1].

Figure 1 shows that the rate that a contaminant is swept out of a city by the winds can vary by a factor of four or more due to solar heating variations from day to night and due to variations in the relative strength of the wind gusts. The horizontal axis of the figure indicates the relative strength of the gusting fluctuations at the boundaries, from about 20% on the left to about 100% on the right. For each of six different "environmental" conditions, twelve ground-level sources were released, four independent realizations at each of three source locations around the urban geometry. These source locations and the scale lengths of all the wind fluctuations were held fixed for the six different runs. The value of the exponential decay time in minutes is plotted for each source and realization as a diamond-shaped symbol. The figure shows that the decay time is two or three times longer for release at night compared to the day for otherwise identical conditions. The dark blue diamonds (decay times) should be compared with the light blue and the purple diamonds compared with the red. One can also see that the decay times get systematically shorter as the wind fluctuation amplitude is increased from left to right. This is emphasized by the light blue shaded bar through the center of the four daytime data sets.

*3.1.3 Tree Effects*

Although we can resolve individual trees if they are large enough, their effects (i.e., aerodynamic drag, introduction of velocity fluctuations, and heat losses) are represented through modified forest canopy models [24] including effects due to the presence of foliage. For example, an effective drag-force source term for the momentum equations can be written as, $\mathbf{F} = -C_d a(z) |\mathbf{v}| \mathbf{v}$, where $C_d$ =0.15 is an isotropic drag coefficient, a(z) is a seasonally-adjusted leaf area density, z is the vertical coordinate, and $\mathbf{v}$ is the local velocity. The foliage density is represented in a fractal-like way so that fluctuations will appear even in initially laminar flows through geometrically regular stands of trees.

*3.1.4 Turbulent Backscatter*

The distribution of subgrid-scale (SGS) viscosity is a distinct feature characterizing the ability of different LES models to capture the underlying unresolved physics, ranging from purely dissipative scalar to tensorial scale-similarity models. An overall positive SGS viscosity implies that energy is transferred from resolvable flow structures towards small, unresolved scales via a cascade process (outscatter). Conversely a negative SGS viscosity implies that energy is overall transferred in the opposite direction by a reverse cascade process, i.e. backscatter – which can become important in complex geometries such as involved in CT when a large amount of turbulent kinetic energy is present in the *unresolved* scales. Even when the systematic, overall cascade corresponds to outscatter, backscatter, both systematic and stochastic, can occur at select wavelengths and for certain nonlinear triads of modes. Modeling how the unresolved features of the flow contribute to the large scales through this (stochastic) backscatter process presents a difficult challenge: how are these effects to be predicted based on the resolvable scale information?

Because of the anisotropic features of the implicit SGS modeling incorporated [15], MILES offers an effective approach for the simulation of inherently inhomogeneous turbulent flows in complex geometries such as involved in CT. It has been demonstrated that this SGS modeling is not purely dissipative, and that some degree of desirable systematic backscatter is actually incorporated implicitly in MILES [15]. Additional (explicit) backscatter effects can be modeled by taking advantage of the flux-limiter information computed by the FCT convection algorithms.

For each component of the fluid momentum, the unused high order flux is accumulated at each grid point during the direction-split convection stages of the integration, and is measured in terms of its absolute value summed over all three directions for each timestep and suitably normalized by the density, i.e.,

$$\varepsilon = \left[ \sum (1 - \phi) \left| \Delta \mathbf{v}_f^H - \Delta \mathbf{v}_f^L \right| \right] / \langle \rho \rangle .$$

The flux limiter $\phi$ is described more fully in section 4 below. This quantity is plotted in Figs. 2 and 3 for several cross-sections from a FAST3D-CT simulation of the airflow over Washington DC.

Figure 2 shows three horizontal planes sliced through the FAST3D-CT grid at constant k indices. These planes are spaced 3 cells apart and indicate the magnitude of the stochastic backscatter velocities at 3 meters (upper right), 21 meters (center) and 39 meters (lower left) off the ground. Red colors indicate an average 10 cm/sec effective subgrid flow speed and faster, yellow indicates about 3 cm/sec and black indicates about 1 cm/sec.

When the FCT algorithm detects structure in the flow that it "knows" cannot be resolved on the grid, only a fraction of the anti-diffusion flux can be applied. The fraction that cannot be used is an implicit estimate of this unresolved flow and it is coupled on the grid scale to the specifics of the fluid dynamic convection algorithm. This estimate is an inexpensive replacement for the multi-scale filtering schemes used in many of the current LES approaches. Furthermore, since the eddy dissipation has already been included in the (anisotropic) MILES representation with a suitable tensorial form, these unused fluxes are available for other, higher order corrections.

Figure 3 shows eight vertical planes sliced through the FAST3D-CT grid, four north-south planes at constant i indices and four east-west planes at constant j indices. These planes are spaced 25 cells (150 meters) apart. The quantity plotted is again the magnitude of the SGS flux □ defined above. The blue band adjacent to the upper boundary of the grid is a region where the imposed boundary flow is sufficiently laminar that the stochastic flux is quite small.

Note the effect of building wakes in generating the unused fluxes and also note that the vortex shedding from buildings tends to carry this turbulence about two building heights into the air. This is a nighttime computation so the atmosphere is stabilized due to thermal stratification. Note also that some subgrid activity can be noted away from the buildings due undoubtedly to nonlinear cascade in the atmospheric turbulence being convected with the flow.

FAST3D-CT uses these "stochastic back scatter fluxes" by pseudo-randomly perturbing the resolved flow velocity in each cell by an amount proportional (with a factor of about 0.3) to the unused flux velocities depicted in the figs 2 and 3. In some geometries, these additional grid-scale fluctuations break symmetries and initiate three-dimensional instabilities via stochastic backscatter that other wise would have to grow up from computer round-off. They also transport small particles and droplets to material surfaces as a result of unresolved turbulence even though the resolved flow field has a zero velocity normal to the walls. This means that particles and droplets can deposit on a ceiling as well as a floor. Finally, the numerical limiting of the imposed stochastic fluctuations, caused by the nonlinear flux limiter, provides a small additional macroscopic (resolved scale) transport right where the FCT algorithm has detected subgrid structure. Each of these potentially realistic effects requires further theoretical analysis and/or a phenomenological model carefully calibrated by experiment. This work remains to be done

All MILES, and more generally ILES, methods are quite capable of capturing (at least semi-quantitatively) how much unresolved, small-scale structure is actually present from looking at the evolving resolved-scale solutions. Further, systematic diffusion of the eddy transport type can be automatically left in the flow, but the fluctuating, driving effects of random-phase, unresolved small-scale motions scattering back onto the large scales are missing unless specifically included as a subgrid phenomenology. Therefore it is our continuing interest to employ the unused fluxes with random, or stochastic, multipliers. However, a factor of two increase in the spatial resolution of LES and MILES models will most likely bring more improvement in the accuracy of the well resolved scales than subgrid models will ever provide regardless of the type of LES employed. Work is ongoing to provide satisfying proofs of these statements.

*3.1.5 Geometry Specification*

An efficient and readily accessible data stream is available to specify the building geometry data to FAST3D-CT. High-resolution (1 m or smaller) vector geometry data in the ESRI ARCVIEW data format is commercially available for most major cities. From these data, building heights are determined on a regular mesh of horizontal locations with relatively high resolution (e.g., 1 m). Similar tables for terrain, vegetation, and other land use variables can be extracted. These tables are interrogated during the mesh generation to determine which cells in the computational domain are filled with building, vegetation, or terrain. This masking process is a very efficient way to convert a simple geometric representation of an urban area to a computational grid.

This grid masking approach is used to indicate which computational cells are excluded from the calculation as well as to determine where suitable wall boundary conditions are to be applied. However, the grid masking approach is too coarse to represent rolling terrain, for which a shaved cell approach is used instead. The terrain surface is represented by varying the location of the lower interface of the bottom cell. Even though this results in a terrain surface that is discontinuous, the jump between adjacent cells is small, and operational results show that that this approach works reasonably well and is far better than the grid masking approach for representing terrain.

A more accurate representation of the geometry is possible with the VCE approach [25] in which the cell volume and interface areas are allowed to vary. This level of detail now begins to approach that of conventional aerodynamics CFD and it remains to be seen if this is necessary.

*3.1.6 Wall Boundary Conditions*

Appropriate wall boundary conditions must be provided so that the airflow goes around the buildings. It is not possible with theavailable resolution to correctly model the boundary layer on the surface. Therefore, rough-wall boundary layer models [26] are used for the surface stress, i.e., $\tau = \rho C_D (U_{//})^2$, and for the heat transfer from the wall, $H_o = \rho C_p C_H U_{//} (\theta - \theta_o)$, where $\rho$ is the mass density, $C_D$ and $C_H$ are coefficients characterizing the roughness and thermal properties of the walls or ground surface, $U_{//}$ is the tangential velocity at the near-wall (first grid point adjacent to the wall), Cp is the specific heat at constant pressure, and $\theta$ and $\theta_o$ are the potential temperature at the wall, and near-wall, respectively.

## 4. MILES Implicit SGS model

Historically, flux-limiting (flux-correcting) methods have been of particular interest in the MILES context. A flux-limiter $0 \le \psi \le 1$ combines a high-order convective flux-function $\mathbf{v}_f^H$ that is well behaved in smooth flow regions, with a low-order dispersion-free flux-function $\mathbf{v}_f^L$ that is well behaved near sharp gradients. Thus the total flux-function with the limiter $\psi$ becomes $\mathbf{v}_f = \mathbf{v}_f^H - (1-\psi)[\mathbf{v}_f^H - \mathbf{v}_f^L]$. Properties of the implicit SGS model in MILES are related to the choice of $\psi$, $\mathbf{v}_f^L$, and $\mathbf{v}_f^H$, as well as to other specific features of the algorithm [15,16]. This is quite similar to choosing/adjusting an (explicit) SGS model in the context of conventional LES.

Because of its inherently less-diffusive nature, prescribing $\psi$ based on local monotonicity constraints is a more attractive choice in developing MILES [14-16]. This is supported by our comparative channel flow studies [16] of the global performance of MILES as a function of flux limiter. For example, the van-Leer TVD limiter (e.g., [27]) was found to be too diffusive as compared to FCT [19] and GAMMA [28] limiters which produce velocity profiles that agree well with the reference DNS data.

### *4.1 Street Crossings*

Another approach to controlling unwanted numerical diffusion is through the appropriate choice of low and high order transport algorithms. In our simulations of urban areas, the typical grid resolution is of the order of 5 to 10 meters. While this resolution is adequate to represent the larger features of the city, many of the smaller features are resolved with only one to two cells. This is true of smaller streets found in cities, which are about 20 m wide. Alleyways are even smaller. These smaller streets aremay be represented by only one or two cells in our computation, putting a tremendous demand on the numerical convection not to diffuse and retard the flow down these narrow streets.

By using the rough-wall boundary conditions discussed above instead of no-slip boundary conditions, the flow can proceed unhampered down a single street even for streets that are only one cell wide. However, if there is another street intersecting the first, it was found that the flow essentially stagnates at this intersection. The problem only occurs when dealing with streets which are 1–2 cells wide and not with wider streets. After careful inspection, it was determined that the problem arose due to the form of the diffusion term in the low-order solution in the standard FCT algorithm, LCPFCT [21], used in the FAST3D-CT code.

The traditional low-order component of FCT introduces numerical diffusion even when the velocity goes to zero (as in the cross street) [21]. In normal situations, the flux limiter is able to locate an adjacent cell that has not been disturbed by the diffusion in the low-order method and is able to restore the solution to its original undiffused value. However, when the streets are 1–2 cells wide, the region of high velocity is diffused by low-order transport and there are no cells remaining at the

higher velocity (Fig. 4). Thus the flux limiter cannot restore the solution in these cells to the original high value.

A solution to this problem lay in changing the form of the diffusion in the low-order method. In LCPFCT, The algorithmic diffusion coefficient for the low-order scheme is given by $\mu = \frac{1}{6} + \frac{1}{3}\mu$, where the Courant number $\mu = |U|\Delta t / \Delta x$. Note that $\mu$ does not go to zero even when U goes to zero (as in the cross street). The simplest less-diffusive low-order algorithm which ensures monotonicity is the upwind method previously used in the formal MILES analysis (e.g., [16]) for which the diffusion coefficient is given by $\mu_{upwind} = \frac{1}{2}|\mu|$, which has the desired form for $\mu$. When the diffusion coefficient in the low-order component of FCT is replaced by $\mu_{upwind}$, the flow no longer stagnates at the intersection of streets (Fig. 4). This variation of the low-order method is only used for the momentum equations. It is not required for the density equation, since the density is almost constant everywhere. With this modification of the low-order method, the global properties of the transport algorithm were altered sufficiently to address this problem peculiar of under-resolved flows in urban areas.

## 5. Practical Examples

### *5.1 Gaussian Lagrangian vs. Unsteady-3D Solutions*

Gaussian atmospheric transport and dispersion schemes are characterized by some initial direct spreading of the contaminant upwind by the diffusion, regardless of wind speed. The characteristic differences between the three Gaussian similarity solutions in fig. 5 are similar to the differences between different Gaussian plume/puff models. None of these approximate, idealized solutions has the correct shape, trapping behavior, or plume width when compared to the FAST3D-CT simulation shown in the upper-right panel of the fig. 5. The contaminant gets trapped in the re-circulation zones behind buildings and continues to spread laterally long after simpler models say the cloud has moved on.

More detailed comparisons using actual "common use" puff/plume models (e.g., [29]) show a range of results depending on how much of the 3D urban boundary layer information from the detailed simulation is incorporated in the Gaussian model. Though building-generated aerodynamic asymmetries cannot be replicated, crosswind spreading and downwind drift can be approximately matched given enough free parameters. However, because the detailed simulations show that the plume expands like an angular sector away from the source, Gaussian models show too rapid a lateral spreading in the vicinity of the source to provide a plume that is approximately the correct width downwind.

### *5.2 Unsteady-3D Solution – Chicago*

The city of Chicago is typical of a large, densely populated metropolitan area in the United States. The streets in the downtown area are laid out in a grid–like fashion, and are relatively narrow. The buildings are very tall but with small footprints. For example, the Sears tower is now the tallest building in the U. S.

Figures 6–8 show different views of a contaminant cloud from a FAST3D-CT simulation of downtown Chicago using a 360 x 360 x 55 grid (6 m resolution). A 3 m/s wind off the lake from the east blows contaminant across a portion of the detailed urban geometry data set required for accurate flow simulations. One feature that is very apparent from these figures is that the contaminant is lofted rapidly above the tops of the majority of the buildings. This vertical spreading of the contaminant is solely due to the geometrical effect of the buildings. This behavior has also been observed in other simulations in which the buildings are not as tall.

Placement of the contaminant source can have a very nonlinear effect on the dispersion characteristics. Figures 9 and 10 show results of identical simulations with the exception of the contaminant release locations, which are shown by the red markers. The blue markers show the release location in the other simulation. Although the release locations differed by less than 0.5 km the dispersion characteristics are markedly different. The narrower dispersion pattern in fig. 9 is likely caused by a channeling effect of the Chicago River where velocities are higher. The wider dispersion pattern in fig. 10 is likely due to a combination of flow deflection and recirculation of the flow from the building geometry. This behavior may also be dependent on release time. Work is continuing to determine the function dependence on location and release time. However, it is clear that bulk parameterizations of urban surface characteristics will be unable to account for these nonlinear effects.

Additional simulations for Chicago were used to examine the effect of the modified low-order component of FCT as described in section 4.1. Figure 11 shows the contaminant at ground level 9 minutes after release using the standard FCT algorithm

LCPFCT [21]. The channeling effect of the Chicago River is quite dominant, though some lateral spreading occurs as well. The calculations were then repeated with the modified low-order method. These results are shown in Fig. 12. It is immediately apparent that the lateral spreading is much larger in this case and that the cloud also propagates more rapidly downstream. These effects can be attributed to the lowered numerical diffusion in the cross-stream direction and the consequent lowering of numerical diffusion overall. Figure 13 shows the velocity (averaged horizontally over the computational domain) and RMS fluctuation profiles for both LCPFCT and the modified low-order scheme. The modified method has higher values for both velocity and RMS fluctuation. This is consistent with the observation of increased downstream and cross-stream propagation of the contaminant.

While it is expected that the solution with the lower numerical diffusion is preferable, in the absence of experimental measurements, it is not possible to directly assess this improvement.

### *5.3 Unsteady-3D solution – Baghdad*

Baghdad is rather typical of capital cities - it has large, spread-out governmental buildings, parks and monuments. There is no large dense urban core with tall buildings (there are several 20+ story buildings that are spread out). Residential areas are mostly suburban with some high-rise housing. This city structure is quite different from Chicago with its skyscrapers. A limited amount of high-resolution building data was available from a government-related source; however this data only included the largest buildings and covered a fraction of the area of the city. Large portions, especially residential areas, were not covered. Also, land-use data (trees, water, etc.) were not available in high- resolution form.

The missing data was constructed manually, primarily from commercially available satellite photographs of the city. These photographs had sufficient resolution to discern trees, water, and even types of housing. "Synthetic" buildings were generated to represent areas not covered by the available high-resolution data. Typical building heights and shapes found in suburbs were assigned at random to suburban regions. One of the difficulties not typically found in CFD calculations which proved to be a challenge was to ensure proper geo-referencing of the data, i.e., ensure everything lined up. This is especially severe when working from photographs that do not have a uniform resolution, and may sometimes not have the proper orientation.

#### *5.3.1 In-situ Validation*

One of the obvious difficulties that arise for simulations of urban areas is that of validation of results. Experimental data is rarely available, and what little that is available is extremely limited in scope and coverage. The type and extent of data that is available restrict the quality of the validation effort. For Baghdad, no specific field measurements are available. However, just prior to the start of the war in Iraq, large trenches filled with oil were set ablaze in hope that the smoke would obscure targets. The smoke from one such fire provided an opportunity to at least visually "validate" our plume calculations. Figure 14 is a satellite photograph (courtesy DigitalGlobe) of the smoke from a trench fire near the monument to the Unknown Soldier. Figure 15 and 16 show the results from our simulations of the event. Color contours of the tracer gas are shown. The weather conditions for that day were given as "light wind from northwest." The simulations were carried with nominal wind speed of 3 m/s at 340º. An important unknown that had to be estimated is the level of fluctuation in the wind. The simulation depicted in Fig. 15 used a low level of fluctuation, which is consistent with the light steady winds typically found in March in the area. In order to investigate the importance of wind fluctuations, a higher level of fluctuations was simulated as shwn in fig. 16, which had fluctuations four times as high in aplitude as the baseline case (Fig. 15). As expected, the plume does spread slightly further. However, for low wind fluctuations, the spreading is largely controlled by the geometry of the city – an effect which becomes more dominant in dense urban areas. These calculations show that while a good knowledge of the weather is required for accurate predictions, in order to predict a worst-case scenario it is possible to select the appropriate parameters without perfect knowledge of all input conditions.

## 6. Concluding Remarks

Physically realistic urban simulations are now possible but still require some compromises due to time, computer, and manpower resource limitations. The necessary trade-offs result in sometimes using simpler models, numerical algorithms, and geometry representations than we would wish. We know that

the quality of the spatially and time-varying boundary conditions imposed, that is, the fluctuating winds, require improvement. Detailed time-dependent wind field observations at key locations can be processed suitably to provide initial and boundary conditions and, at the least, can be used for global validation (e.g., [23]).

We believe that the building and large-scale fluid dynamics effects that can be presently captured govern the turbulent dispersion, and expect that the computed predictions will get better in time because the MILES methodology is convergent. However, there is considerable room to improve both the numerical implementation and the understanding of the stochastic backscatter that is included both implicitly and explicitly.

Inherent uncertainties in simulation inputs and model parameters beyond the environmental conditions also lead to errors that need to be further quantified by comparison with high quality reference data. Judicious choice of test problems for calibration of models and numerical algorithms are essential and sensitivity analysis help to determine the most important processes requiring improvement. In spite of inherent uncertainties and model trade-offs it is possible to achieve some degree of predictability.

Testing and calibrating stochastic backscatter algorithms and any theoretical work attending that effort is a difficult task. We would like to suggest a class of test problems for doing this. Figure 7 in Reference [7], shows the convergence of macroscopic entrainment with resolution in a set of MILES simulations performed with FAST3D. This problem was used originally to identify the various numerical effects in MILES and to corroborate the prediction of a minimum in the entrainment at a certain, rather coarse, numerical resolution. The minimum occurs because short wavelengths, that provide some measurable additional entrainment, cannot be resolved near the minimum but the residual numerical diffusion present in high-order FCT (monotone) convection algorithms has become quite small. Therefore increasing resolution actually increases the entrainment. Better LES algorithms, including proposed stochastic backscatter modifications, should reduce the depth of the minimum and push the resolution at the minimum to coarser grids. By revisiting this problem we should be able to extend the quantitative understanding and to calibrate practically the stochastic backscatter model coefficients.

The FAST3D-CT simulation model can be used to simulate sensor and system response to postulated threats, to evaluate and optimize new systems, and conduct sensitivity studies for relevant processes and parameters. Moreover, the simulations can constitute a virtual test range for micro- and nano-scale atmospheric fluid dynamics and aerosol physics, to interpret and support field experiments, and to evaluate, calibrate, and support simpler models.

Figure 7 illustrates the critical dilemma in the CT context: unsteady 3D urban-scenario flow simulations are currently feasible – but they are still expensive and require a degree of expertise to perform. First responders and emergency managers on site for contaminant release threats cannot afford to wait while actual simulations and data post-processing are being carried out. A concept addressing this problem [1,30] carries out 3D unsteady simulations in advance and pre-computes compressed databases for specific urban areas based on suitable (e.g., historical, seasonally adjusted) assumed weather, wind conditions, and distributed test-sources. The relevant information is summarized as *dispersion nomograph*™ data so that it can be readily used through portable devices, in conjunction with urban sensors providing current observational information regarding local contaminant concentrations, wind speed, direction, and relative strength of wind fluctuations.

## Acknowledgments

The authors wish to thank Bob Doyle and Ted Young for helpful technical discussions and scientific contributions to this effort. Aspects of the work presented here were supported by ONR through NRL, the DoD High Performance Computing Modernization Office, DARPA and MDA.

## References

[1] Boris, J.P.; 2002, "The Threat of Chemical and Biological Terrorism: Preparing a Response", Comp. Science and Engineering, **4**, pp 22-32.

[2] "Hazard Prediction and Assessment Capability", http://www.dtra.mil/td/acecenter/td_hpac_fact.html.

[3] Bauer, T. and Wolski M., 2001, "Software user's Manual for the Chemical/Biological Agent Vapor, Liquid, and Solid Tracking (VLSTRACK) Computer model, Version 3.1," NSWCDD/TR-01/83, April 2001.

[4] ALOHA Users Manual, 1999. Available for download at: http://www.epa.gov/ceppo/cameo/pubs/aloha.pdf Additional information http://response.restoration.noaa.gov/cameo/aloha.html.

[5] Leone, J.M, J.S. Nasstrom, D.M. Maddix, D.J. Larsen, and G. Sugiyama, 2001, “LODI User’s Guide, Version 1.0”, Lawrence Livermore National laboratory, Livermore CA.
[6] Aliabadi, S. and Watts, M.; 2002, ”Contaminant Propagation in Battlespace Environments and Urban Areas,” AHPCRC Bulletin, Vol 12, Number 4, in http://www.ahpcrc.org/publications/archives/v12n4/Story3/).
[7] S. Chan. 1994. FEM3C – An Improved Three-Dimensional Heavy-Gas Dispersion Model: User’s Manual”, UCRL-MA-116567 Rev. 1, Lawrence Livermore National laboratory, Livermore CA.
[8] F.Camelli and R. Löhner. 2003, “Assessing Maximum Possible Damage for Release Events”. Seventh Annual George Mason University Transport and Dispersion Modeling Workshop, June 2003.
[9] Sagaut P., 2002, “Large Eddy Simulation for Incompressible Flows”, Springer, New York.
[10] F.F. Grinstein & G.Em Karniadakis; 2002, Editors, “Alternative LES and Hybrid RANS/LES”; J. Fluids Engineering, **124**, pp. 821-942.
[11] Boris J.P.; 1989, “On Large Eddy Simulation Using Subgrid Turbulence Models”, in *Whither Turbulence? Turbulence at the Crossroads*, J.L. Lumley Ed., Springer, New York, p 344.
[12] J.P. Boris, F.F. Grinstein, E.S. Oran, and R.J. Kolbe, “New Insights into Large Eddy Simulation“, Fluid Dynamics Research, 10, 199-228 (1992).
[13] E.S. Oran and J.P. Boris (1993) “Computing Turbulent Shear Flows - A Convenient Conspiracy”, Computers in Physics **7**(5): 523-533, September-October 1993.
[14] C. Fureby and F.F. Grinstein, “Monotonically Integrated Large Eddy Simulation of Free Shear Flows”, AIAA Journal, 37, 544-556 (1999).
[15] C. Fureby and F.F. Grinstein, "Large Eddy Simulation of High Reynolds-Number Free & Wall-Bounded Flows", Journal of Computational Physics, 181, 68 (2002).
[16] Grinstein F.F. and Fureby C., Recent Progress on MILES for High Reynolds-Number Flows, Journal of Fluids Engineering, 124, 848 (2002).
[17] Cybyk, B.Z., J.P. Boris, T.R. Young, C.A. Lind and A.M. Landsberg; 1999, “A Detailed Contaminant Transport Model for Facility Hazard Assessment in Urban Areas”, AIAA Paper 99-3441.
[18] Cybyk, B.Z., J.P. Boris, T.R. Young, M.H. Emery and S.A. Cheatham; 2001, “Simulation of Fluid Dynamics Around Complex Urban Geometries”, AIAA Paper 2001-0803.
[19] J.P. Boris and D.L. Book, "Flux-Corrected Transport I, SHASTA, A Fluid Transport Algorithm that Works", Journal of Computational Physics, 11, 8-69 (1973).
[20] Boris, J. P., and Book, D. L. (1976) Solution of the Continuity Equation by the Method of Flux-Corrected Transport. *Methods in Computational Physics* 16: pp. 85-129.
[21] Boris, J. P., A.M. Landsberg, E.S. Oran and J.H. Gardner (1993) LCPFCT - A Flux-Corrected Transport Algorithm for Solving Generalized Continuity Equations. U.S. Naval Research Laboratory Memorandum Report NRL/MR/6410-93-7192.
[22] Mayor, S.D., Spalart, P.R., and Tripoli, G.J.; 2002, “Application of a Perturbation Recycling Method in the Large-Eddy Simulation of a Mesoscale Convective Internal Boundary Layer”, J. Atmos. Sci., 59, 2385.
[23] Bonnet, J.P., Coiffet, C., Delville, J., Druault, Ph., Lamballais, E., Largeau, J.F., Lardeau, S., and Perret, L.;2002, “The Generation of Realistic 3D Unsteady Inlet Conditions for LES”, AIAA 2003-0065.
[24] M.J. Dwyer, E.G. Patton, and R.H. Shaw, Boundary-Layer Meteorology, **84**, 23-43 (1997).
[25] A.M. Landsberg, T.R. Young, and J.P. Boris, "An Efficient Parallel Method for solving Flows in Complex Three-Dimensional Geometries", AIAA Paper 94-0413 (1994).
[26] S.Pal Arya,“Introduction to Micrometeorology”, Academic Press, 1988.
C.;[27] C. Hirsch, 1999, “Numerical Computation of In-ternal and External Flows”, J. Wiley and Sons.
[28] Jasak H., Weller H.G., and Gosman A.D.; 1999, “High Resolution NVD Differencing Scheme for Arbitrarily Unstructured Meshes”, Int. J. Numer. Meth. Fluids, 31, 431.
[29] J. Pullen, J.P. Boris T.R. Young, G. Patnaik, and J.P. Iselin, “Comparing Studies of Plume Morphology using a Puff Model and an Urban High-Resolution Model,” Seventh Annual George Mason University Transport and Dispersion Modeling Workshop, June 2003.
[30] J.P. Boris, K. Obenschain, G. Patnaik, and T.R. Young (2002) “CT-ANALYST™, Fast And Accurate CBR Emergency Assessment”, Proceedings of the 2nd International Conference on Battle Management, Williamsburg, VA, 4-8 November 2002.

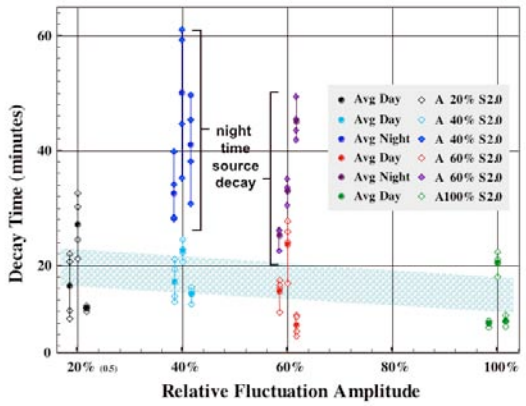


Figure 1. Effect of fluctuations on trapping of contaminants.

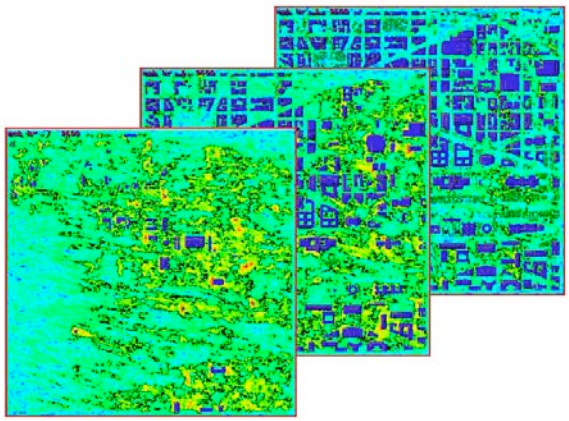

Figure 2. Magnitude of stochastic backscatter velocities along horizontal planes.

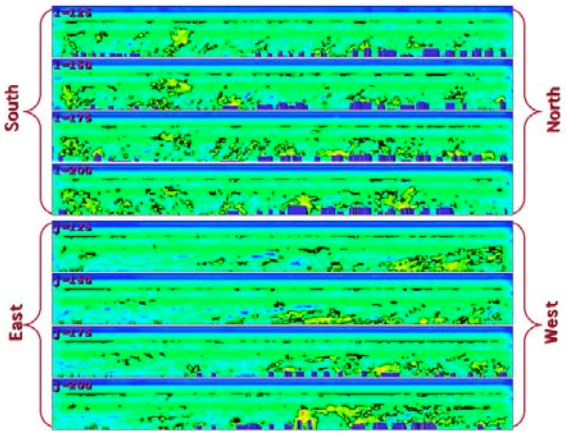


Figure 3. Magnitude of stochastic backscatter velocities along vertical planes.

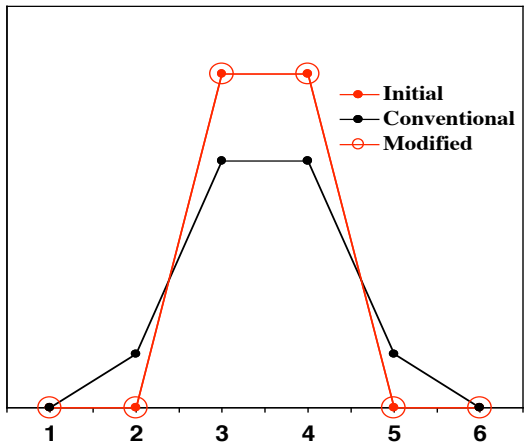


Figure 4. Advected quantity as function of grid index for both the conventional and modified low-order schemes.

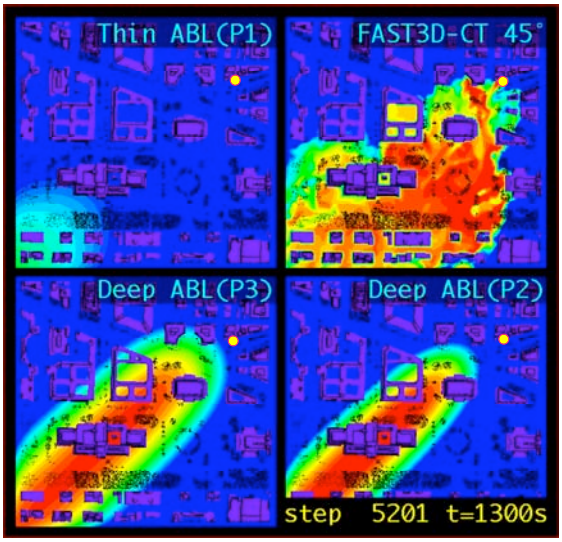


Figure 5. Comparison of Gaussian Plume and FAST3D-CT simulations.

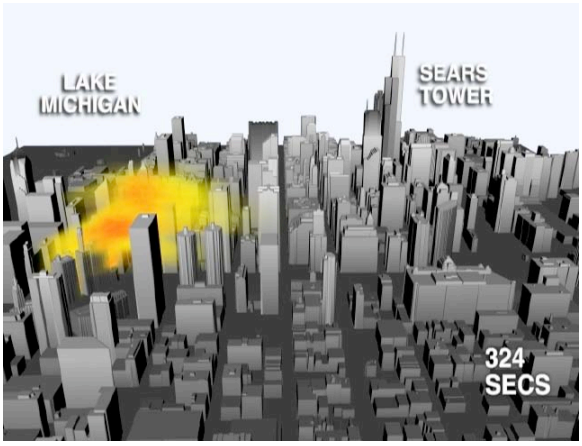


Figure 6. View of contaminant release looking East toward downtown Chicago.

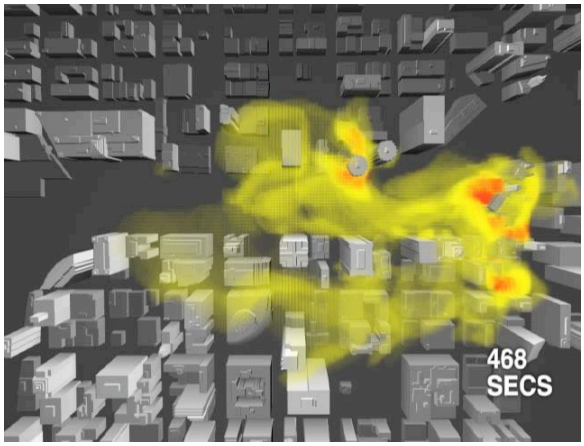


Figure 7. Overhead view of contaminant concentrations over Chicago River.

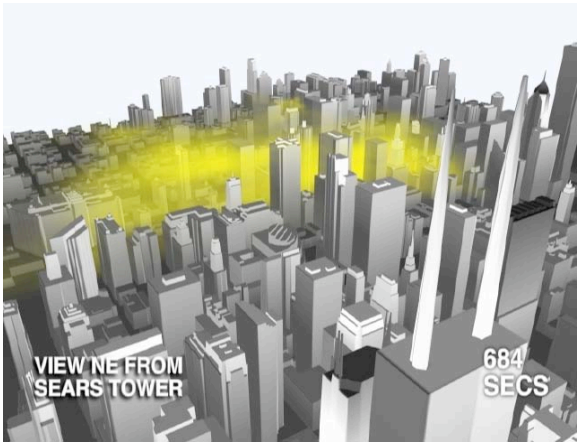


Figure 8. View of contaminant from the Sears tower

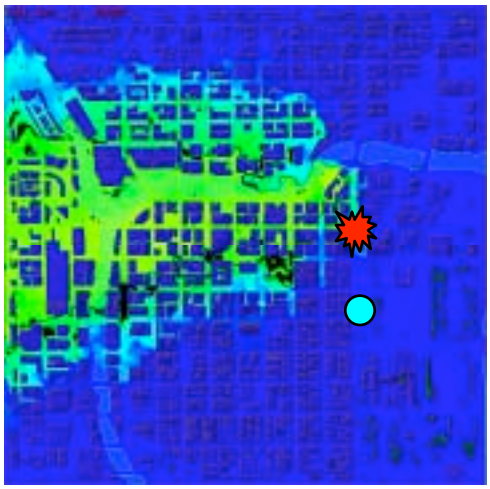

Figure 9. Contaminant dispersion at ground level for release close to Chicago River. = Active source.

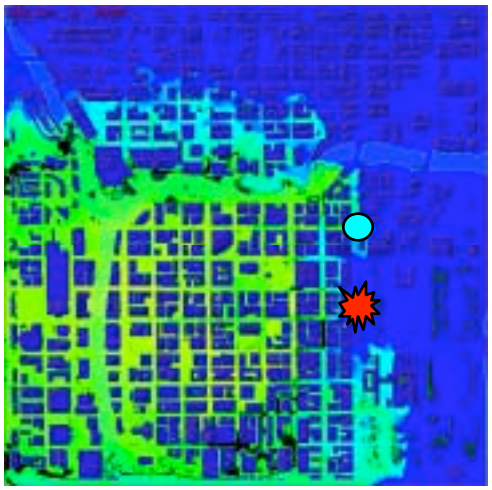

Figure 10. Contaminant dispersion at ground level for release further from Chicago River.

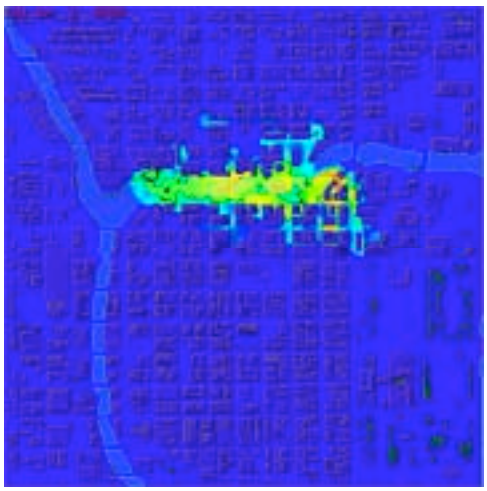

Figure 11. Contaminant dispersion using standard low-order method.

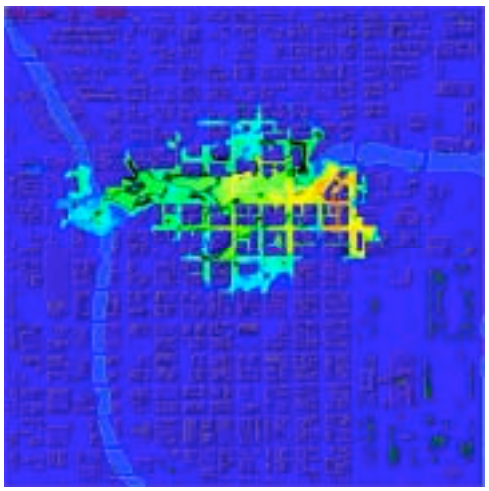

Figure 12. Contaminant dispersion using modified low-order method.

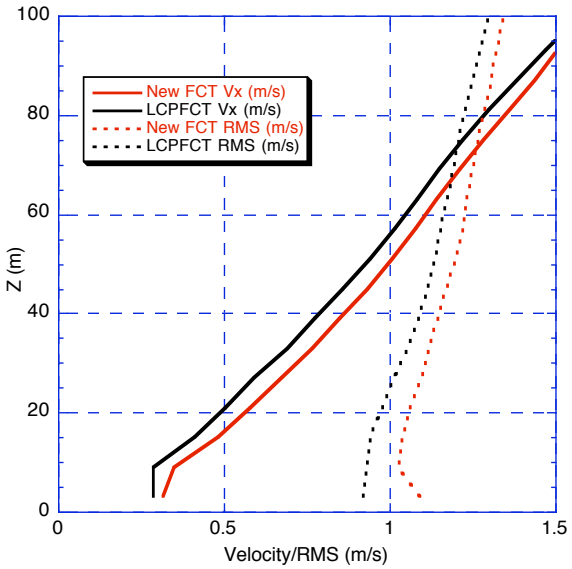


Figure 13. Comparison of the standard and modified low-order method velocity and RMS fluctuation profiles.

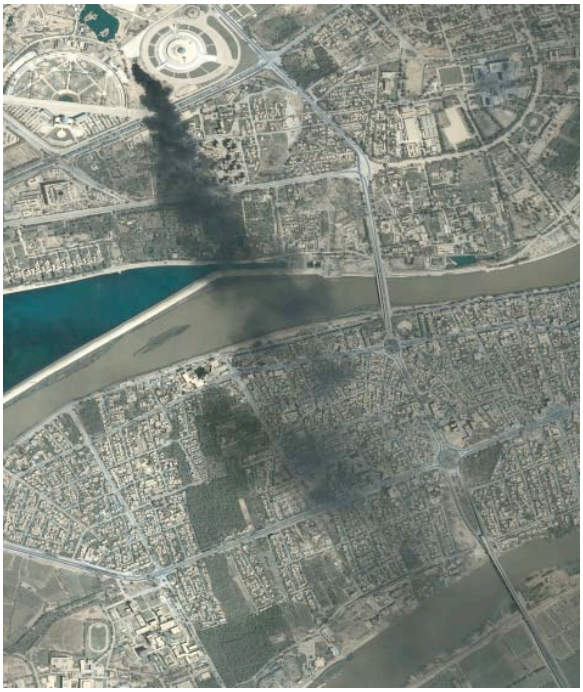

Figure 14. Smoke plume from oil fire in Baghdad.

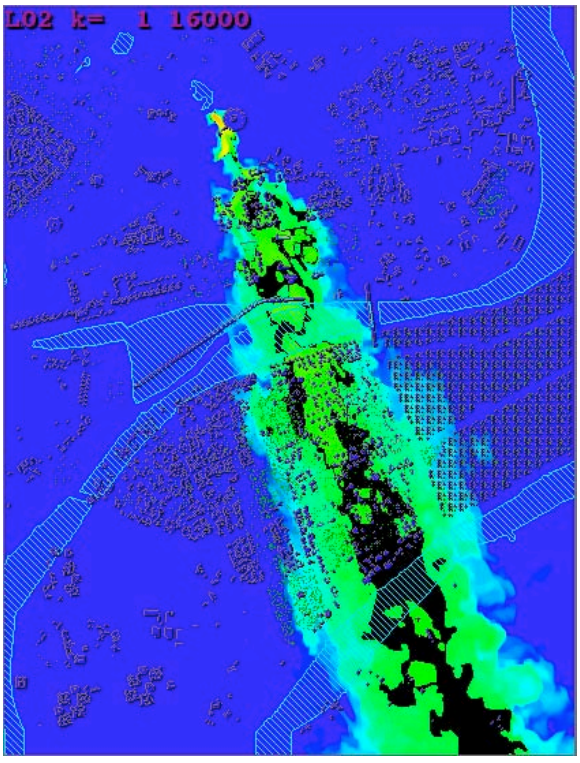


Figure 15. Simulation of smoke plume. Low wind fluctuations.

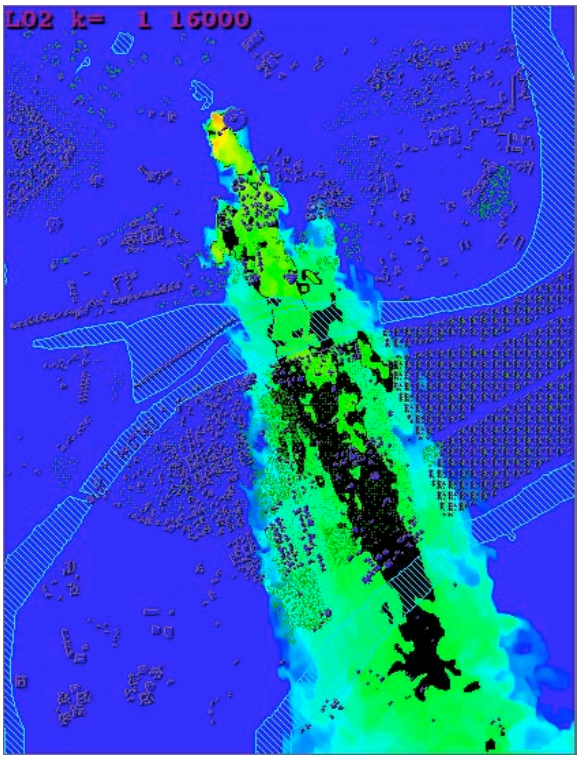


Figure 16. Simulation of smoke plume. High wind fluctuations.